Optical Communications and Quantum Optics

Academic and Research Staff
Professor Jeffrey H. Shapiro, Dr. Franco N. C. Wong, Dr. Vittorio Giovannetti, Dr. Lorenzo Maccone

Graduate Students
Marius A. Albota, Joe Aung, Shane M. Haas, Eser Keskiner, Christopher E. Kuklewicz, Elliott J. Mason, Emily W. Nelson

Introduction
The central theme of our programs has been to advance the understanding of optical and quasi-optical communication, radar, and sensing systems. Broadly speaking, this has entailed: (1) developing system-analytic models for important optical propagation, detection, and communication scenarios; (2) using these models to derive the fundamental limits on system performance; and (3) identifying, and establishing through experimentation the feasibility of, techniques and devices which can be used to approach these performance limits.

Quasi-Phase Matched Nonlinear Optics

Sponsors
MIT Lincoln Laboratory
Contract BX-7156

Project Staff
Dr. Franco N. C. Wong, Elliott J. Mason

Quasi-phase matching (QPM) [1,2] in periodically poled ferroelectric crystals such as lithium niobate is an important technique for nonlinear frequency generation because it allows efficient operation at any user-specified wavelength within the transparency window of the material. Ease of fabrication, large nonlinearity, and room-temperature noncritically phase-matched geometry make periodically-poled nonlinear crystals the material of choice in many applications. Potential device applications include channel frequency conversion and signal amplification for dense wavelength division multiplexed (DWDM) optical communication networks.

We have made substantial improvements in our fabrication of periodically-poled lithium niobate (PPLN). We have developed a number of fabrication procedures such as accurate lithography of short-period gratings (~6-8 µm), wet etching of spin-on-glass and fused silica coating. We have extensively tested various combination of electrodes (Ti/Au and NiCr) and resist materials for producing optimal metal grating structures. A computer model [3] was implemented for predicting optimal poling voltages based on the crystal wafer geometry and grating periods. New mask designs were made to prevent domain merging for short- to medium-period gratings. As a result of these new fabrication procedures, we were able to obtain gratings with 6.5-µm periods, although grating uniformity and domain merging still needed improvement. Also, Elliott Mason visited Martin Fejer's group at Stanford for two weeks to learn and discuss some of the finer details of PPLN fabrication [4,5].

The actual poling step involved the application of a high voltage pulse to the wafer that required a good control of the amount of charges to be transferred to the wafer. In this area, we have upgraded the computer acquisition hardware and improved the software codes for an automated poling process with a 1% accuracy in the charge transfer. Coupled with our computer model of the poling process, the new system was capable of controlling the voltage ramp-up and ramp-down to prevent dynamic shock, improving nucleation population at the beginning of the pulse for domain seeding, and hence more uniform poling, and adjusting voltage levels for sharp turn-on and turn-off of poling currents without breakdown.

As a result of our systematic study of various factors in the fabrication and poling procedures, we have obtained greater consistency in our poled samples with better yield and grating uniformity. We have even compared our samples with those purchased from Deltronic (20 µm gratings), and found that our samples had greater grating uniformity and conversion efficiency.

We have also applied the periodic poling technique to barium magnesium fluoride ($BaMgF_4$) [6,7] which is a promising candidate as a nonlinear crystal for deep UV generation due to its transparency and high damage threshold. It has a small nonlinear coefficient and birefringent phase matching is not available for second harmonic generation of deep UV radiation. We were successful in poling $BaMgF_4$ with grating periods of 19.2 and 21.1 µm. The required poling voltage was found to be 16-18 kV/mm, which is slightly lower than that of lithium niobate, the most widely used periodically-poled material for near-IR generation. Unlike lithium niobate, etching periodically-poled $BaMgF_4$ did not reveal its periodic structure. Instead we have used the Environmental Scanning Electron Microscope on campus for imaging the poled crystal with good results. Scott Buchter at Lincoln Laboratory obtained second harmonic generation of 266 nm by third-order quasi-phase matching using a sample of $BaMgF_4$ with a 19.2-µm grating. He showed that the conversion efficiency was within 50% of the expected value of the nonlinear *d* coefficient of 0.03 pm/V, subject to large uncertainties in the actual value of the nonlinear coefficient, the correct grating period for optimal quasi-phase matching, and the quality of the grating. Potential applications for periodically poled $BaMgF_4$ include inspection and sensing for next generation optical lithography in the deep UV region.

Quantum Information and Communication

Sponsors
Army Research Office
Contract DAAD19-00-1-0177
MIT Lincoln Laboratory
Contract BX-7466
National Reconnaissance Office
Contract NRO-000-00-C-0032
National Reconnaissance Office
Contract NRO-000-00-C-0158

Project Staff
Prof. Jeffrey H. Shapiro, Dr. Franco N. C. Wong, Dr. Vittorio Giovannetti, Dr. Lorenzo Maccone, Marius A. Albota, Joe Aung, Eser Keskiner, Christopher E. Kuklewicz, Elliott J. Mason, Emily W. Nelson

We have embarked on new research in the area of quantum information technology whose goal is to enable the quantum-mechanical information transmission, storage, and processing needed for future applications in quantum computing and quantum communication. Our theoretical work in this area has focused on architectural designs for long-distance teleportation. Of particular interest to us has been the identification of high-performance means for generating the polarization-entangled photons needed for many quantum information applications, including teleportation, super-dense coding, and entanglement-based quantum cryptography.

Theory The preeminent obstacle to the development of quantum information technology is the difficulty of transmitting quantum information over noisy and lossy quantum communication channels, recovering and refreshing the quantum information that is received, and then storing it in a reliable quantum memory. Together with Professor Seth Lloyd and Dr. Selim Shahriar of RLE, and Dr. Phillip Hemmer of the Air Force Research Laboratory, we have proposed and analyzed a novel architecture for the singlet-state approach to quantum teleportation. A simple block diagram of this architecture is shown in Fig. 1. It consists of an ultrabright narrowband source of polarization-entangled photons pairs (*P*), connected to a pair of trapped Rb atom quantum memories (*M*) by *L*-km-long lengths of standard telecommunication fiber.

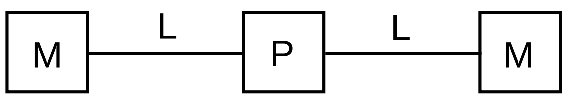

Figure 1. Schematic of long-distance quantum communication system: *P* = ultrabright narrowband source of polarization-entangled photon pairs; *L* = *L* km of standard telecommunication fiber; *M* = trapped atom quantum memory.

Each *M* block in Fig. 1 is a quantum memory in which a single ultracold ^{87}Rb atom is confined by a CO_2-laser trap in an ultra-high vacuum chamber with cryogenic walls within a high-finesse single-ended optical cavity. An abstract representation of the relevant hyperfine levels for such a memory is given in Fig. 2(a). A 795 nm photon in an arbitrary polarization can be absorbed, transferring the qubit from the photon to the degenerate *B* levels of Fig. 2(a), and thence to long-lived storage levels, by coherently driving the *B*-to-*D* transitions. By means of optically-off-resonant (OOR) transitions, the Bell states of two atoms in a single vacuum-chamber trap can be converted into superposition states of one of the atoms. All four Bell measurements needed for the Bennett *et al*. singlet-state teleportation process [8] can then be made, sequentially, by detecting the presence (or absence) of fluorescence as an appropriate sequence of OOR laser pulses is applied to the latter atom. The Bell-measurement results (two bits of classical information) in one memory can be sent to a distant memory, where (at most) two additional OOR pulses are needed to complete the state transformation process. More details on this memory, and its use in teleportation, are given in [9].

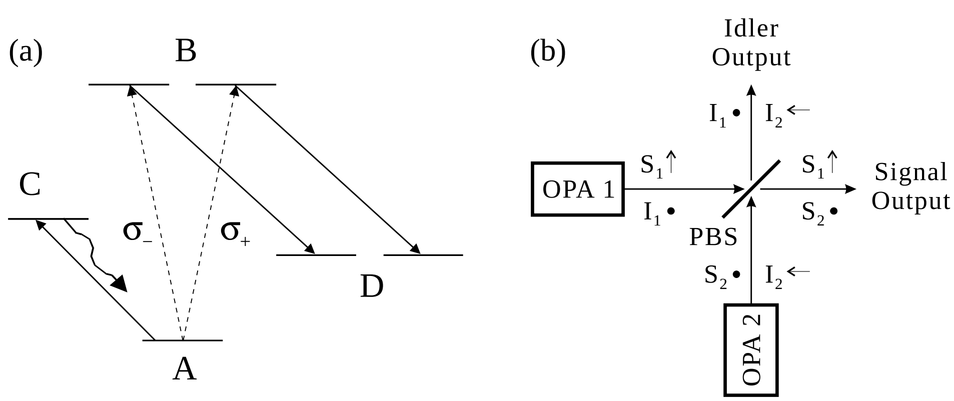

Figure 2. Essential components of singlet-state quantum communication system from Fig. 1. Left (a), simplified atomic-level schematic of the trapped Rb atom quantum memory: *A*-to-*B* transition occurs when one photon from an entangled pair is absorbed; *B*-to-*D* transition is coherently driven to enable storage in the long-lived *D* levels; *A*-to-*C* cycling transition permits nondestructive determination of when a photon has been absorbed. Right (b), ultrabright narrowband source of polarization-entangled photon pairs: each optical parametric amplifier (OPA1 and OPA2) is type-II phase matched; for each optical beam the propagation direction is *z*, and *x* and *y* polarizations are denoted by arrows and bullets, respectively; PBS, polarizing beam splitter.

The *P* block in Fig. 1 is an ultrabright narrowband source of polarization-entangled photon pairs [10], capable of producing ~10^6 pairs/sec in ~30 MHz bandwidth by appropriately combining the signal and idler output beams from two doubly-resonant type-II phase matched optical parametric amplifiers (OPAs), as sketched in Fig. 2(b). The importance of our resonant approach to entanglement generation is the need to achieve high flux within the narrow linewidth of the Rb atom memory; existing parametric downconverter sources of entanglement are far too broadband to permit useful transmission rates in the Fig. 1 architecture. As detailed below, we are presently working to demonstrate OPA entanglement sources.

For long-distance transmission to remotely-located memories, in the Fig. 1 architecture, we generate the entangled photon pairs in the 1550-nm-wavelength low-loss window of standard telecommunication window, and then employ quantum frequency conversion [11,12] to shift the entanglement to the 795 nm wavelength needed for the Rb atom memory, see Fig. 3.

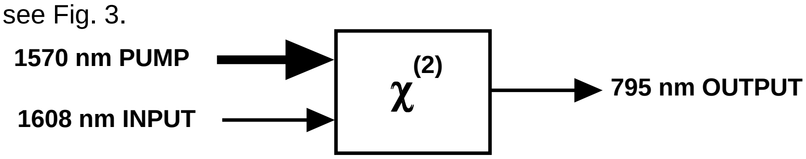

Figure 3. Schematic of quantum frequency conversion: a strong pump beam at 1570 nm converts a qubit photon received at 1608 nm (in the low-loss fiber transmission window) to a qubit photon at the 795 nm wavelength of the ^{87}Rb quantum memory.

Transmission in the 1550-nm-wavelength window is not enough to make the Fig. 1 singlet-state architecture compatible with standard telecommunication fiber. It is also crucial to ensure that polarization is not degraded by the propagation process. Our scheme for polarization maintenance, shown in Fig. 4, relies on time-division multiplexing. By transmitting non-overlapping time slices from the signal beams from our

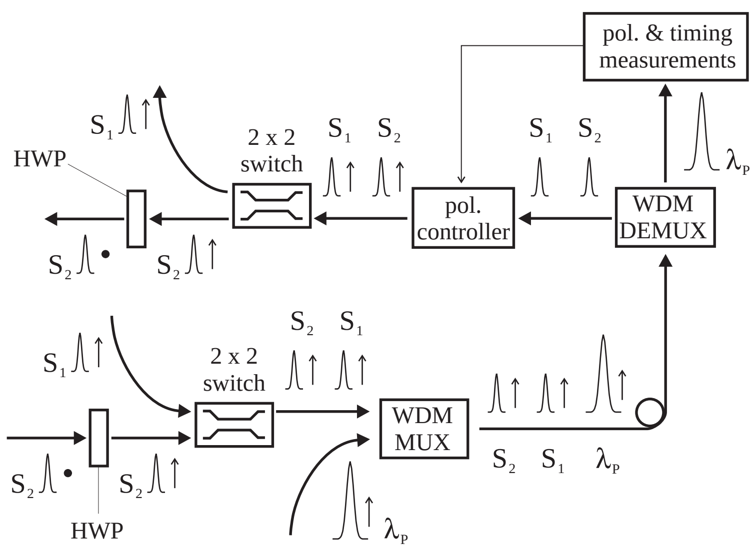

Figure 4. Transmission of time-division multiplexed signal beams from OPA1 and OPA2 through an optical fiber. With the use of a half-wave plate (HWP) the signal pulses and the pilot pulse are linearly polarized the same way. The pilot pulse — at wavelength λ_p which is different from the signal or idler wavelengths — is injected into and extracted from the fiber using a wavelength-division multiplexer (WDM MUX) and a wavelength-division demultiplexer (WDM DEMUX), respectively. Not shown is the final polarizing beam splitter for combining the two signal-beam outputs, cf. Fig. 2(b). A similar overall arrangement is used to transmit the idler beams from OPA 2 to OPA2.

two OPAs — along with a strong pilot pulse — down the fiber in a common linear polarization, we can use polarization tracking on the pilot pulse to obtain the information needed to restore the linear polarizations of the two signal-beam time slices. These are then combined, after half-wave plate polarization rotation and delay compensation, to recover the desired vector signal beam. A similar procedure is used for the idler outputs from the two OPAs travelling down the other fiber. In effect, this replaces the source-located passive PBS in Fig. 2(b) with a time-gated memory-located polarization combiner at the far end of each fiber. This approach, which is inspired by the Bergman et al. two-pulse fiber squeezing experiment [13], common-modes out the vast majority of the phase fluctuations and the polarization birefringence incurred in the fiber, permitting standard telecommunication fiber to be used in lieu of the lossier and much more expensive polarization-maintaining fiber.

Quantum communication is carried out in the Fig. 1 configuration via the following protocol. The entire system is clocked. Time slots of signal and idler (say 400 ns long) are transmitted down optical fibers to the quantum memories. These slots are gated into the memory cavities — with their respective atoms either physically displaced or optically detuned so that no A-to-B absorptions occur. After a short loading interval (a few cold-cavity lifetimes, say 400 ns), each atom is moved (or tuned) into the absorbing position and B-to-D coherent pumping is initiated. After about 100 ns, coherent pumping ceases and the A-to-C cycling transition (shown in Fig. 2(a)) is repeatedly driven (say 30 times, taking nearly 1 μs). By monitoring a cavity for the fluorescence from this cycling transition, we can reliably detect whether or not a 795 nm photon has been absorbed by the atom in that cavity. If neither atom or if only one atom has absorbed such a photon, then we cycle both atoms back to their A states and start anew. If no cycling-transition fluorescence is detected in either cavity, then, because we have employed enough cycles to ensure very high probability of detecting that the atom is in its A state, it must be that both atoms have absorbed 795 nm photons and stored the respective qubit information in their long-lived degenerate D levels. These levels are not resonant with the laser driving the cycling transition, and so the loading of our quantum memory is nondestructively verified in this manner.

We expect that the preceding memory-loading protocol can be run at rates as high as R = 500 kHz. With a high probability, P_{erasure}, any particular memory-loading trial will result in an erasure, i.e., propagation loss and other inefficiencies combine to preclude both atoms from absorbing photons in the same time epoch. With a small probability, P_{success}, the two atoms will absorb photons from a single polarization-entangled pair, *viz*., we have a memory-loading success. With a much smaller probability, P_{error}, both atoms will have absorbed photons but these photons will not have come from a single polarization-entangled pair; this is the error event. These probabilities constitute a complete taxonomy of the loading-trial possibilities, i.e., their respective probabilities sum to unity.

Using the dual-OPA entanglement source's quantum statistics that we derived in [10], we have performed a cold-cavity loading analysis for the quantum memory to evaluate the key figures of merit for the Fig. 1 configuration: throughput and fidelity [14]. Our singlet-state quantum communication architecture enjoys a robustness to propagation losses and other inefficiencies in that these effects merely increase P_{erasure} and hence reduce throughput, i.e., the number of successful entanglement-loadings/sec, $N_{\text{success}} = RP_{\text{success}}$, that could be achieved if the quantum memories each contained a lattice of trapped atoms for sequential loading of many pairs. It is the loading errors, which occur with probability P_{error}, that provide the ultimate limit on the entanglement fidelity of the Fig. 1 configuration. This loss-limited fidelity is given by $F_{\max}= 1 - P_{\text{error}}/2(P_{\text{success}} + P_{\text{error}})$, where we have assumed that the error event loads independent randomly-polarized photons into each memory. In Fig. 5 we have plotted the throughput and loss-limited fidelity for our quantum communication system under the following assumptions: OPAs pumped at 1% of their oscillation thresholds; 5 dB of excess loss in each P-to-M block path in Fig. 1; 0.2

dB/km loss in each fiber; memory-cavity linewidth equal to one half the source-cavity linewidth; and R = 500 kHz memory cycling rate. We see from this figure that a throughput of 200 pairs/sec can be sustained out to an end-to-end path length ($2L$) of 50 km, with a loss-limited fidelity of 97.5%.

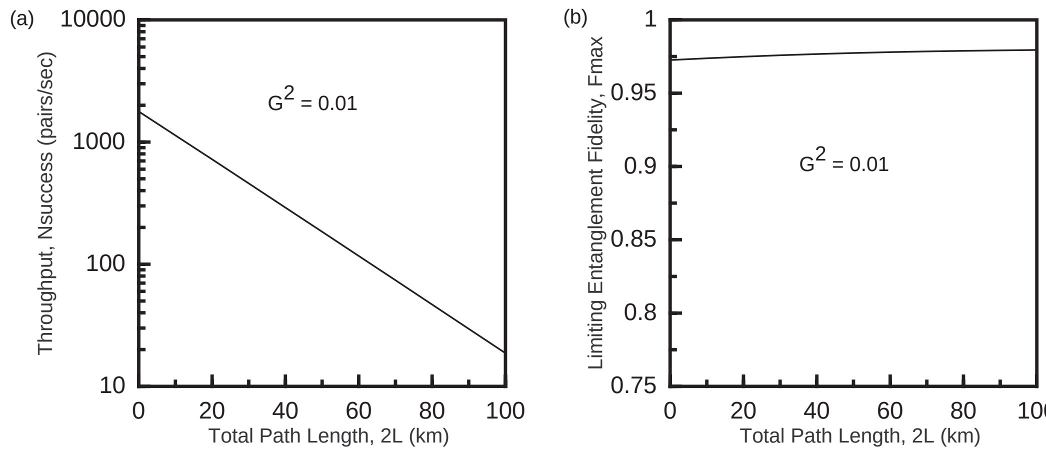

Figure 5. Figures of merit for Fig. 1 configuration. Left (a), throughput, N_{success}, vs. total path length, $2L$. Right (b), limiting entanglement fidelity, $F_{\max}$, vs. total path length, $2L$.

<u>Experiment</u> A parametric downconverter can be used to produce pairs of entangled photons, but the resulting low rate of photon-pair generation has hindered proof-of-principle experiments. This problem is exacerbated if the photon pairs are to transfer their entanglement to a trapped-atom quantum memory, because the relevant pair-generation rate becomes that for photons within the bandwidth of the memory's high-Q optical cavity. The best narrowband pair-generation rate, for a parametric downconverter, can be inferred to be at most 15 s^{-1}, within a 30-MHz bandwidth at 702-nm wavelength, using 150 mW of pump power and very high numerical-aperture optics [15].

We have recently shown, theoretically, that the signals and idlers from a pair of optical parametric amplifiers (OPAs) can be combined to produce an ultrabright source of narrowband polarization-entangled photons [10]. For OPAs using periodically-poled potassium titanyl phosphate (PPKTP), we estimate that the pair production rate is 1.5 x 10^6 s^{-1} within a 30-MHz bandwidth at a 795-nm center wavelength using only 10 mW of pump power. Many quantum information applications will be enabled by development of such a low-power, ultrabright source of entangled photon pairs.

We have set up a bulk-KTP doubly-resonant OPA in a single-ended standing-wave cavity configuration. With ~100 µW of pump power at 532 nm, we observed a singles count rate of 10^4 s^{-1} using a Si single-photon counter that had a quantum efficiency of ~1% at the OPA output wavelength of 1064 nm, thus yielding an estimated pair production rate of 10^6 s^{-1} [16]. The output consisted of three components: broadband nonresonant mode pairs, narrowband singly resonant mode pairs, and narrowband doubly resonant mode pairs.

The nonresonant mode pairs are similar to those obtained with spontaneous parametric downconversion without cavity enhancement. The nonresonant output was necessarily broadband with a bandwidth equal to the downconversion fluorescence spectrum, which was about 100 GHz in our experiment for a 1-cm-long KTP crystal. For the singly resonant output, the downconverted signal field was resonant with the cavity but not the idler field or vice versa. Hence, the singly resonant output was narrowband with a bandwidth given by the cavity linewidth of ~30 MHz. This resonant mode occurred every free spectral range (5.5 GHz) over the fluorescence spectrum. The doubly-resonant mode pair output was present when the cavity was tuned to resonance with both signal and idler fields, with a double-Lorentzian cavity linewidth of ~20 MHz. Because of the double resonance requirement, there was usually only one doubly-resonant mode pair over the entire fluorescence spectrum.

Figure 6 shows the singles count in 10-ms measurement time bins of the OPA output as the cavity length was scanned. These data were taken with 3 mW of pump power. The observed resonance peaks are similar to those of the outputs of a doubly resonant optical parametric oscillator (OPO) [17], and matching the predicted separation of ~9 nm between peaks. The singly-resonant output did not exhibit such resonances because it could be continuously tuned, which can be an advantage. We estimated that the percentages of the nonresonant, singly resonant, and doubly resonant mode pairs to be 65%, 19%, and 16%, respectively.

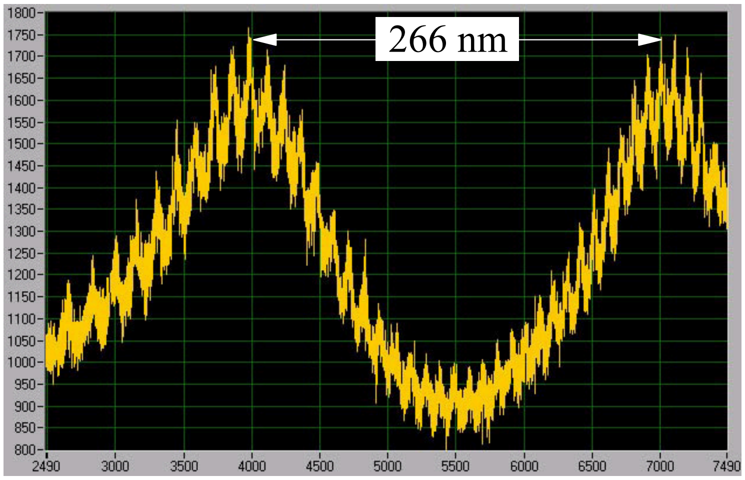

Figure 6. Trace of detected singles count as cavity length is swept.

The signal and idler outputs from the type-II phase matched KTP OPA were orthogonally polarized. The outputs were rotated by a half-wave plate before entering a polarizing beam splitter and were detected in separate single-photon detectors. We have made measurements of the coincidence counts as we varied the measurement time duration with (a) no polarization rotation and (b) 45° polarization rotation, as shown in Fig. 7. For large time bins, the positive slope of the coincidence counts is due to accidental Poisson coincidences (we note that the individual signal and idler photon streams had Poisson statistics.) For short times, the coincidences drop off because the signal and idler photons did not emerge from the cavity at the same time. The intercepts at zero time bin give a good estimate of the true coincidence count rates for the OPA outputs. In Fig. 7, the coincidence counts in 5 s are ~43 for 0° polarization rotation and ~13 for 45° rotation. For the singly resonant and doubly resonant outputs, they were mostly, if not all, frequency nondegenerate and hence the polarizing beam splitter acted as a 50/50 beam splitter after the 45° polarization rotation. In this case, we would expect a coincidence count reduction of 50%, or 21.5 in 5 s. The lower number of coincidences in Fig. 7(b) of 30% is due to quantum interference of the nonresonant photon pairs. These broadband signal and idler photons were frequency degenerate and hence they could be represented by the state $|HV\rangle + |VH\rangle$. After the 45° polarization rotation, in the new polarization basis, the nonresonant mode pair could be denoted by $|HH\rangle + |VV\rangle$, which implies that coincidences for this mode should vanish. Given the estimated 65% of the OPA output was the nonresonant mode, a complete quantum interference of this mode should have yielded only 7.5 coincidences in 5 s. The higher observed number indicates there was only partial quantum interference, limited by angle walkoff of the KTP crystal and uncertainties in our measurements due to the detectors' low quantum efficiencies.

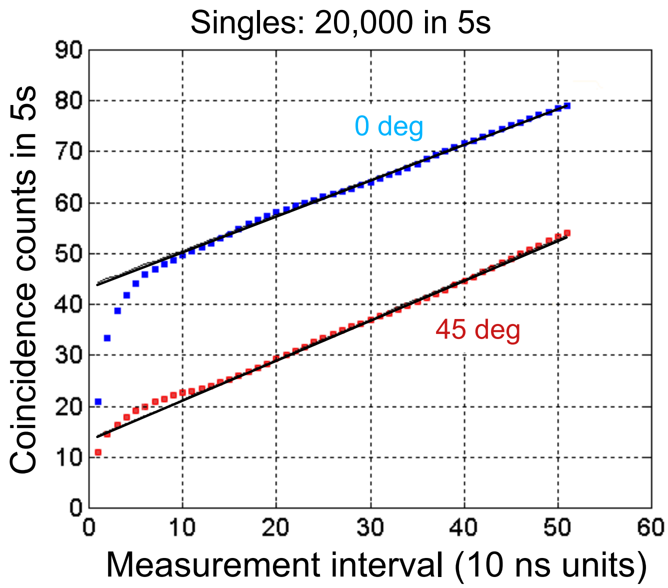

Figure 7. Coincidence counts vs. measurement time bins for (a) 0° polarization rotation and (b) 45° polarization rotation.

Due to the low quantum efficiencies of the Si detectors at 1064 nm, we have begun constructing a 397.5-nm pumped OPA system using a PPKTP crystal with outputs at 795 nm that matches the wavelength of the trapped ^{87}Rb quantum memory. We have also started setting up a PPLN OPA system that would generate entangled photons at 795 nm and 1.61 µm. Besides being wavelength tunable, the PPLN OPA would allow the 1.61 -µm photons to be transported to remote locations via low-loss optical fibers.

Atmospheric Optical Communications

Sponsors
Defense Advanced Research Projects Agency
Grant MDA972-00-1-0012

Project Staff
Prof. Jeffrey H. Shapiro, Dr. Franco N. C. Wong, Shane M. Haas

In future battlefield operations, communications and data networking will play a much more significant role. Properly designed optical communication systems operating over atmospheric paths may be able to provide covert, high burst rate communications with the necessary quick set up and tear down capability. Laser beams propagating through the atmosphere are subject to a wide variety of deleterious effects, including absorption, depolarization, beam spread, angular spread, multipath spread, Doppler spread, and fading. These effects, which represent the combined impact of the atmosphere's molecular constituents, entrained aerosols and hydrometeors, and turbulence-induced refractive index fluctuations, may drastically curtail the performance of an atmospheric optical link. We have recently begun a program, in collaboration with Prof. Vincent Chan of the Laboratory for Information and Decision Systems, to: provide understanding of battlefield optical communication applications and their implied demands on optical systems; develop architectural constructs that are attainable, but make maximum use of device and subsystem capability to achieve high overall performance; and develop and demonstrate key system concepts in an experimental test bed facility.

The central thrust of this new program will be to address the effects of atmospheric turbulence and how it may be mitigated through the use of diversity techniques in space, time, and frequency. In theoretical work, we have begun to study the use of space-time coding (STC) for turbulence mitigation. An STC system uses multiple transmit and receive antennas to combine temporal and spatial diversity. Tarokh *et al*. [18] have established design criteria of space-time codes for the Rayleigh and Ricean fading channels that are encountered in wireless communications at microwave frequencies. Optical communication through atmospheric turbulence is a lognormal-fading channel. We have shown [19] that a subset of these previous codes minimize the pairwise error probability for the lognormal channel. Our approach extends to other fading channels with zero-mean, statistically independent path gains. In our experimental work, we have begun to assemble a diversity-communication test bed, using commercially available OC-48 lasers and detectors. The resulting 2.5 GHz link will be tested over a 500 m outdoor path under a variety of propagation conditions. Both transmitter and receiver diversity techniques will be explored.

References

1. M. M. Fejer, G. A. Magel, D. H. Jundt, and R. L. Byer, “Quasi-phase-matched second harmonic generation: tuning and tolerances,” IEEE J. Quantum Electron. **28**, 2631-2654 (1992).

2. M. Yamada, N. Nada, M. Saitoh, and K. Watanabe, “First-order quasi-phase matched $LiNbO_3$ waveguide periodically poled by applying an external field for efficient blue second-harmonic generation,” Appl. Phys. Lett. **62**, 435-4362 (1993).

3. G. D. Miller, “Periodically poled lithium niobate: modeling, fabrication, and nonlinear-optical performance,” Ph.D. thesis, Stanford University, 1998.

4. L. E. Myers, R. C. Eckardt, M. M. Fejer, R. L. Byer, W. R. Bosenberg, and J. W. Pierce, “Quasi-phase matched optical parametric oscillators in bulk periodically poled $LiNbO_3$,” J. Opt. Soc. Am. B **12**, 2102-2116 (1995).

5. R. G. Batchko, V. Y. Shur, M. M. Fejer, and R. L. Byer, “Backswitch poling in lithium niobate for high-fidelity domain patterning and efficient blue light generation,” Appl. Phys. Lett. **75**, 1673-1675 (1999).

6. P. S. Bechthold and S. Haussühl, “Nonlinear optical properties of orthorhombic barium format and magnesium barium fluoride,” Appl. Phys. **14**, 403-410 (1997).

7. S. C. Buchter, T. Y. Fan, V. Liberman, J. J. Zayhowski, M. Rothschild, A. Cassanho, H. P. Jenssen, E. J. Mason, and J. H. Burnett, “Periodically poled $BaMgF_4$ for ultraviolet frequency generation,” Postdeadline paper CPD23, Conference on Lasers and Electro-Optics, Baltimore, MD, May 6-11, 2001.

8. C. H. Bennett, G. Brassard, C. Crépeau, R. Josza, A. Peres, and W. K. Wootters, “Teleporting an unknown quantum state via dual classical and Einstein-Podolsky-Rosen channels,” Phys. Rev. Lett. **70**, 1895-1899 (1993).

9. S. Lloyd, M. S. Shahriar, J. H. Shapiro, and P. R. Hemmer, “Long distance, unconditional teleportation of atomic states via complete Bell state measurements,” submitted to Phys. Rev. Lett; preprint quant-ph/0003147.

10. J. H. Shapiro and N. C. Wong, “An ultrabright narrowband source of polarization-entangled photon pairs,” J. Opt. B **2**, L1-L4 (2000).

11. P. Kumar, “Quantum frequency conversion,” Opt. Lett. **15**, 1476-1478 (1990).

12. J. M. Huang and P. Kumar, “Observation of quantum frequency conversion,” Phys. Rev. Lett. **68**, 2153-2156 (1992).

13. K. Bergman, C. R. Doerr, H. A. Haus, and M. Shirasaki, “Sub-shot-noise measurement with fiber-squeezed optical pulses,” Opt. Lett. **18**, 643-645 (1993).

14. J. H. Shapiro, “Long-distance high-fidelity teleportation using singlet states,” to appear in *Quantum Communication, Measurement, and Computing 3*, O. Hirota and P. Tombesi, eds. (Kluwer, New York, 2001); preprint quant-ph/0105055.

15. P. G. Kwiat, E. Waks, A. G. White, I. Appelbaum, and P. H. Eberhard, “Ultrabright source of polarization-entangled photons,” Phys. Rev. A **16**, R773-R776 (1999).

16. E. Keskiner, “An ultrabright narrowband source of polarization-entangled photons,” M.Eng. thesis, Massachusetts Institute of Technology, 2001.

17. D. Lee and N. C. Wong, “Stabilization and tuning of a doubly resonant optical parametric oscillator,” J. Opt. Soc. Am. B **10**, 1659-1667 (1993).

18. V. Tarokh, N. Seshardri, and A. Calderbank, “Space-time codes for high data rate wireless communication: performance criteria and code construction,” IEEE Trans. on Inform. Theory **IT-44**, 744-765 (1998).

19. S. M. Haas, J. H. Shapiro, and V. Tarokh, “Space-time codes for wireless optical communications,” paper to be presented at the 2001 IEEE International Symposium on Information Theory, Washington, D.C.

Publications

J. H. Shapiro and N. C. Wong, “An ultrabright narrowband source of polarization-entangled photon pairs,” J. Opt. B **2**, L1-L4 (2000).

Meeting Papers, Published

1. J. H. Shapiro and N. C. Wong, “An ultrabright narrowband source of polarization-entangled photon pairs,” Digest of Quantum Electronics and Laser Science Conference, San Francisco, CA, May 7-12, 2000.

2. C. Fabre, E. J. Mason, and N. C. Wong, “Self-phase locking in a type II phase-matched optical parametric oscillator,” Digest of Conference on Lasers and Electro-Optics, San Francisco, CA, May 7-12, 2000.

3. J. H. Shapiro, “Long-distance high-fidelity teleportation using singlet states,” to appear in *Quantum Communication, Measurement, and Computing 3*, O. Hirota and P. Tombesi, eds. (Kluwer, New York, 2001); preprint quant-ph/0105055.